

Cu₂ZnSiTe₄: A potential thermoelectric material with promising electronic transport

Himanshu Sharma¹, Bhawna Sahni¹, Tanusri Saha-Dasgupta² and Aftab Alam^{1*}

¹*Department of Physics, Indian Institute of Technology, Bombay, Powai, Mumbai 400 076, India and*

²*Department of Condensed Matter and Materials Physics,
S. N. Bose National Centre for Basic Sciences, JD Block,
Sector III, Salt Lake, Kolkata, West Bengal 700106, India*

(Dated: January 15, 2024)

Transition metal-based quaternary chalcogenides have gathered immense attention for various renewable energy applications including thermoelectrics (TE). While low-symmetry and complex structure help to achieve low thermal conductivity, the TE power factor and hence the figure of merit (ZT) remains low which hinders to promote these class of materials for future TE applications. Here, we investigated the TE properties of a new system, Cu₂ZnSiTe₄, with improved electronic transport using first-principles calculation. The presence of heavy chalcogen like Te, helps to achieve a relatively low bandgap (0.58 eV). This, together with unique electronic band topology, leads to a promising value of power-factor of 3.95(n-type) and 3.06(p-type) mWm⁻¹K⁻² at 900 K. Te atoms also play a crucial role in mixing the optical and acoustic phonon branches which, in turn, are responsible for reduced lattice thermal conductivity (~ 0.7 Wm⁻¹K⁻¹ at high temperature). Though the thermal conductivity is not appreciably low, the electronic transport properties (power factor) are quite favorable to yield promising TE figure of merit (ZT ~ 2.67 (n-type) and ~ 2.11 (p-type) at 900 K). We propose Cu₂ZnSiTe₄ to be a potential candidate for TE applications, and believe to attract future experimental/theoretical studies.

I. Introduction

The limitation of fossil fuel reservoirs and their adverse effects on the environment demands alternate ways of generating renewable energy. Although, there exist several methods of producing renewable energies such as solar, wind or hydro-power etc., yet a large fraction of energy gets wasted in the form of heat while using primary energy resources. Technology based on thermoelectric (TE) devices can help in converting the waste heat into electricity in an eco-friendly manner. Durability over time, zero pollution and no toxic outputs make such devices more useful for renewable energy. These devices require specific types of materials which dictates their efficiency via a thermoelectric figure of merit, defined as $ZT = \frac{S^2\sigma}{\kappa_e + \kappa_l}$, where S , σ , κ_e and κ_l are the Seebeck coefficient, electrical conductivity, electronic and lattice contribution to the thermal conductivity. The inter-coupling of these physical quantities for a given TE material makes it challenging to achieve higher conversion efficiency, and hence the hunt for optimal candidate material remain an ongoing effort in the TE community.

One of the ways to improve efficiency is to optimize the carrier concentration to enhance the power-factor($S^2\sigma$) and hence the figure of merit. Compounds with ultra-low lattice thermal conductivity (κ_l) is yet another strategy to achieve high ZT. The search for materials with such properties has led researchers to a wide variety of materials like clathrates¹, skutterudites², half-heuslers³ and chalcogenides. In particular, chalcogenides have a variety of interesting properties which make them promising for TE applications. Among these, quaternary chalcogenides^{4,5}, especially copper(Cu)-based, have acquired tremendous popularity in the past few years stimulated by their use in several energy related research such as solar cell, magnetoelectric, photocatalysis etc.⁶⁻⁸

In most cases, Cu-based quaternary chalcogenides, with a general formula Cu₂ABX₄, where A is a transition metal, B is group IVA element like Si/Ge/Sn and X is chalcogen, crystallize in a tetragonal structure with space group I42m. The relatively low structural symmetry compare to parent binary compounds and presence of the chalcogen (S, Se, Te) atoms, are known to facilitate low lattice thermal conductivity, thus being attractive for possible TE applications. Quaternary chalcogenides show the lattice thermal conductivity of the order of around 2-3 W/m-K⁹⁻¹² where as binary compounds (ZnS/Se/Te)^{13,14} shows it around 20 w/m-K. Quaternary chalcogenides are also interesting because of the distinct electronic features exhibited by their two structural units (1) the copper-chalcogenide unit being responsible for the electrical transport and (2) ABX₄ unit which remains insulating. Thus, quaternary chalcogenides are potential candidates to optimize the electronic and thermal transport simultaneously and hence achieve higher TE efficiency.

However, most of the reported quaternary chalcogenides are found to show wide band gaps (~ 1 eV), being a hindrance for promising electrical conductivity. Even some of the most studied materials in this family such as Cu₂ASnSe₄ where A=Co,Mn,Cd,Zn show conductivity of the order of 10³-10⁴ Sm⁻¹ lower than their binary counterparts, PbTe and SiGe ($\geq 10^4$ Sm⁻¹)^{10,12,15}. Additionally, the asymmetry associated with structure reduces band degeneracy around the Fermi level and hence degrades the Seebeck coefficient. These result into a moderate value of ZT (~ 0.14 -0.7)^{10,15,16}. Among these compounds, Cu₂CoSnSe₄ (with ZT = 0.7) shows a power-factor of 0.67 mWm⁻¹K⁻² at the intrinsic carrier concentration. Other compounds, e.g. Cu₂(Zn, Cd, Mn)SnSe₄, show even smaller power factor lying in the

range 0.2-0.38 $\text{mWm}^{-1}\text{K}^{-2}$ at ~ 800 K. It has been suggested that non-stoichiometry, such as Cu excess at A/B site in Cu_2ABX_4 , can increase the carrier concentration and hence the electrical conductivity, leading to better power-factor values¹⁷. For example, Cu excess at Mn site in $\text{Cu}_2\text{MnSnSe}_4$ ¹⁸ increases $S^2\sigma$ from 0.38 to 0.7 $\text{mWm}^{-1}\text{K}^{-2}$ and at Cd site in $\text{Cu}_2\text{CdSnSe}_4$ ¹⁶ increases it from 0.16 to 0.5 $\text{mWm}^{-1}\text{K}^{-2}$ resulting in ZT values of 0.61 and 0.65 respectively. Although variation in stoichiometry helps to increase conductivity, the overall enhancement in TE performance is not appreciable. This is partly due to the fact that though this strategy increases σ , it concurrently reduces the Seebeck coefficient and increases the electronic thermal conductivity. Thus, it is very essential to seek alternative means to enhance the electrical conductivity, together with optimizing the carrier concentration in such a way to achieve a reasonable Seebeck coefficient and thermal conductivity in these family of compounds.

Here, we propose $\text{Cu}_2\text{ZnSiTe}_4$ to be a promising candidate in this family for both n-type and p-type conduction. This compound has been synthesized earlier and characterized through X-ray and Raman scattering probes.¹⁹ However, to the best of our knowledge, its electronic and thermal transport properties are never studied, specially from a TE point of view. In this study, we carry out a detailed first principles calculation to evaluate the same. First of all, we show that the inclusion of Tellurium reduces the band gap due to its significant spin-orbit coupling (SOC) effect, enhancing the electrical conductivity. SOC, however, adversely affects the degeneracy of the bands^{20,21} as well, particularly near the valence band, lowering the Seebeck coefficient. As such, a careful optimization of carrier concentration is needed to achieve the optimal value of power factor. To get an estimate of the optimal carrier concentration, we have simulated the TE coefficients in the concentration range 10^{18} - 10^{20} cm^{-3} between 300 and 900 K. A power factor value of $S^2\sigma=3.95$ $\text{mWm}^{-1}\text{K}^{-2}$ is found at 10^{19} cm^{-3} for n-type and $S^2\sigma=3.28$ $\text{mWm}^{-1}\text{K}^{-2}$ at 5×10^{19} cm^{-3} for p-type conduction. Interestingly Te, being a heavy element, also enhances the coupling between optical and acoustic phonon branches causing a reduction in the lattice thermal conductivity. This eventually leads to a high ZT value of 2.67 for n-type and 2.11 for p-type, at 900 K. Thus, $\text{Cu}_2\text{ZnSiTe}_4$ offers promising electronic transport with relatively low lattice thermal conductivity. The present study is expected to motivate future experimental research on this compound as a promising candidate for TE applications.

II. Computational Details

First-principles calculations were performed using density functional theory (DFT) as implemented in Vienna Ab initio Simulation Package (VASP) with the projector augmented wave (PAW) method.²²⁻²⁴ Generalized gradient approximation (GGA) exchange-correlation functional parametrized by Perdew-Burke-Ernzerhof

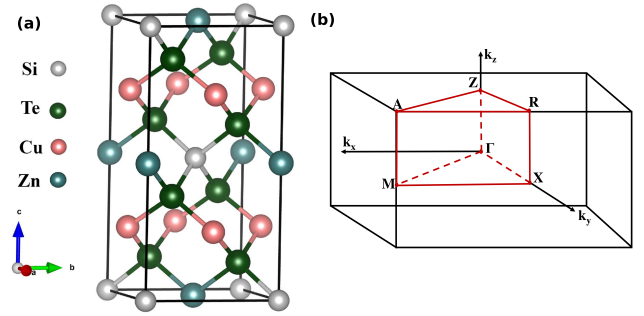


FIG. 1. For bulk $\text{Cu}_2\text{ZnSiTe}_4$, (a) crystal structure with space group $I\bar{4}2m$ and (b) corresponding Brillouin zone

(PBE)²⁵ was used to calculate the electronic structure including spin-orbit coupling (SOC) effect. To make an accurate estimate of the band gap, the modified Becke-Johnson (mBJ)²⁶ meta-GGA exchange-correlation functional including SOC was employed. A plane wave energy cut-off of 500 eV is used with Γ -centred k-mesh to sample the entire Brillouin zone (BZ), with an energy convergence of 10^{-6} eV. We used density functional perturbation theory (DFPT)²⁷ as implemented within VASP for phonon dispersion calculation.²⁸ A dense $20 \times 20 \times 10$ k-mesh was used to check the dynamical stability. To go beyond quasi-harmonic approximation, Phono3py²⁹ was used to calculate lattice thermal conductivity which incorporates third-order inter-atomic force constants. A $2 \times 2 \times 2$ supercell was used within the small displacement method (with a displacement criteria of 0.03 Å) which generated 4738 supercells. Phonon-lifetime was calculated using the tetrahedron method involving a dense $24 \times 24 \times 12$ q-mesh in a temperature range of 300 to 900 K. To analyze the nature of chemical bonding between atoms, the crystal-orbital Hamilton-population (COHP) was calculated using LOBSTER code³⁰⁻³² with mBJ exchange-correlation functional. To calculate the electronic transport properties, Ab initio Scattering and Transport (AMSET)³³ code was used which solves the Boltzmann transport equation considering the energy and temperature-dependent relaxation time (see supplementary material (SM)³⁴ for more details on formalism). AMSET captures various kinds of scattering including Acoustic Deformation Potential (ADP), Polar Optical Phonon (POP), Piezoelectric (PIE) and Ionized Impurity (IMP) scattering to determine the variable relaxation time.

III. Results and Discussions

A. Crystal Structure

$\text{Cu}_2\text{ZnSiTe}_4$ is experimentally reported¹⁹ to crystallize in tetragonal symmetry with space group $I\bar{4}2m$ (#121) (D_{2d} point group) and lattice parameter $a = b = 5.961$ Å and $c = 11.788$ Å at room temperature¹⁹. Figure 1(a,b) shows the crystal structure and its corresponding

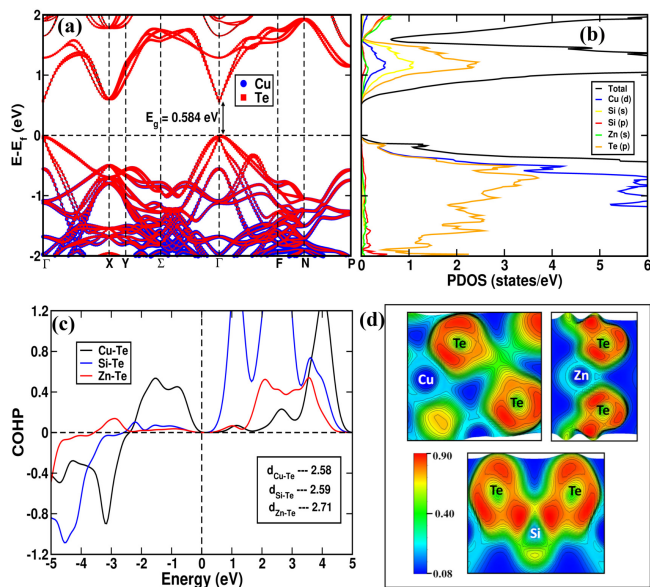


FIG. 2. For $\text{Cu}_2\text{ZnSiTe}_4$, (a) Cu- and Te-projected electronic band structure, (b) orbital projected density of states (PDOS) using mBJ exchange-correlation functional including spin orbit coupling. (c) calculated crystal orbital Hamilton population (COHP) and (d) Electron Localization function (ELF) for Cu-Te, Si-Te and Zn-Te pairs.

Brillouin zone with the high symmetry points. Our theoretically optimized lattice parameters are $a = b = 6.05 \text{ \AA}$ and $c = 11.99 \text{ \AA}$, which agrees fairly well with the experiment values with a mismatch of $\sim 1.4 \%$ in a -axis and $\sim 1.7 \%$ in c -axis. It has two formula units leading to 16 atoms in the unit cell. The structure can be derived starting from a zinc-blend (ZnS) type-structure by making a supercell along the z -direction and replacing zinc with three different cations (Cu, Zn and Si) and Sulphur (S) with tellurium (Te). This makes these quaternary chalcogenides a naturally distorted supercell structure. Every Te (anion) atom is located in a tetrahedral void formed by other cations. Due to the different atomic radii of Cu, Zn and Si, anion (Te) makes three different bonds i.e. $d_{\text{Cu-Te}} = 2.578 \text{ \AA}$ (Cu-Te), $d_{\text{Si-Te}} = 2.586 \text{ \AA}$ and $d_{\text{Zn-Te}} = 2.706 \text{ \AA}$ in the same tetrahedron. In other words, Te forms a locally distorted environment which, in turn, helps in reducing the thermal conductivity.

B. Electronic structure

Figure 2(a,b) shows the electronic band structure and atom/orbital projected density of states (PDOS) of $\text{Cu}_2\text{ZnSiTe}_4$ including the effect of spin orbit coupling. In the absence of SOC, PBE functional yields a band gap of 0.17 eV which gets corrected to 0.74 eV when meta-GGA mBJ functional is used. SOC shows an appreciable effect on the band structure topology (see comparison of band structure with and without SOC in Fig. SI of SM³⁴),

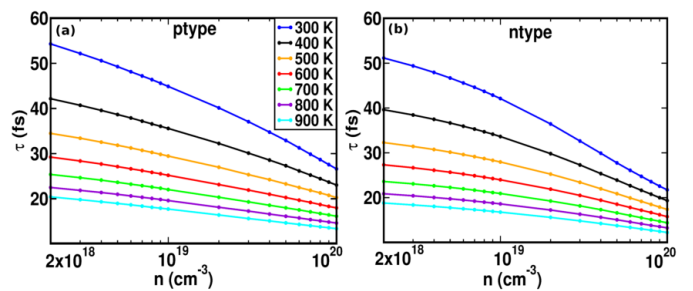


FIG. 3. For $\text{Cu}_2\text{ZnSiTe}_4$, carrier concentration (n) dependence of relaxation time for (a) holes (p-type) and (b) electrons (n-type) at different temperatures.

including a reduction in the band gap value from 0.74 eV to 0.584 eV . Below VBM, bands are relatively flatter compare to CBM implying the possibility of holes becoming the dominant charge carriers in TE transport, which indeed gets reflected in our simulated Seebeck coefficient values (see Sec. D below). Cu and Te atoms together provide the major contribution around valence band maxima (VBM), while Te atoms contribute maximum near conduction band minima (CBM), as is illustrated in the PDOS plot in Fig. 2(b). Further analysis of the PDOS reveals that states below E_F are primarily made up of Cu(d) and Te(p) orbitals, which overlap in the small energy range up to 0.6 eV . Nevertheless, the region above E_F may be separated into two sections: the first includes dominant Te p-orbital, with a minor contribution from Si s-orbital, and the second includes a region between $1.5 - 2.0 \text{ eV}$, which is composed of Zn s-orbital, Te, and Si p-orbital. In other words, this structure can be considered to comprise of two functional units (i) a conduction unit Cu_2Te_4 which dominates at/around E_F and (ii) an insulating unit ZnSiTe_4 away from E_F .

To assess the bonding nature between different atoms, we have simulated the band energy in terms of orbital pair contribution using crystal orbital Hamilton population (COHP) for Cu-Te, Zn-Te and Si-Te bonding interactions. Figure 2(c) shows the COHP vs. energy highlighting the energy-dependent bonding (negative) and anti-bonding (positive) character of different cations and anions in $\text{Cu}_2\text{ZnSiTe}_4$. Since there are no states at Fermi level (E_F), it signifies the stable bonding interaction and semiconducting nature of the compound³⁵. The interaction below the E_F is dominated by Cu-Te pair. This pair shows anti-bonding states due to the localization of charge, as reflected in the charge density plots in Fig. 2(c). Another plausible reason for anti-bonding states near E_F can be the locally distorted structure, as discussed above in the bond length analysis. To further analyze the bonding nature, we have plotted the electron localization function (ELF)³⁶ in Fig. 2(d). A value of $\text{ELF} \sim 1$ indicates a strong localization nature, whereas an electron gas is represented by an ELF of ~ 0.5 . Since the tetrahedral void anion (Te) is linked to various cations (Cu, Zn, and Si), ELF plots are shown

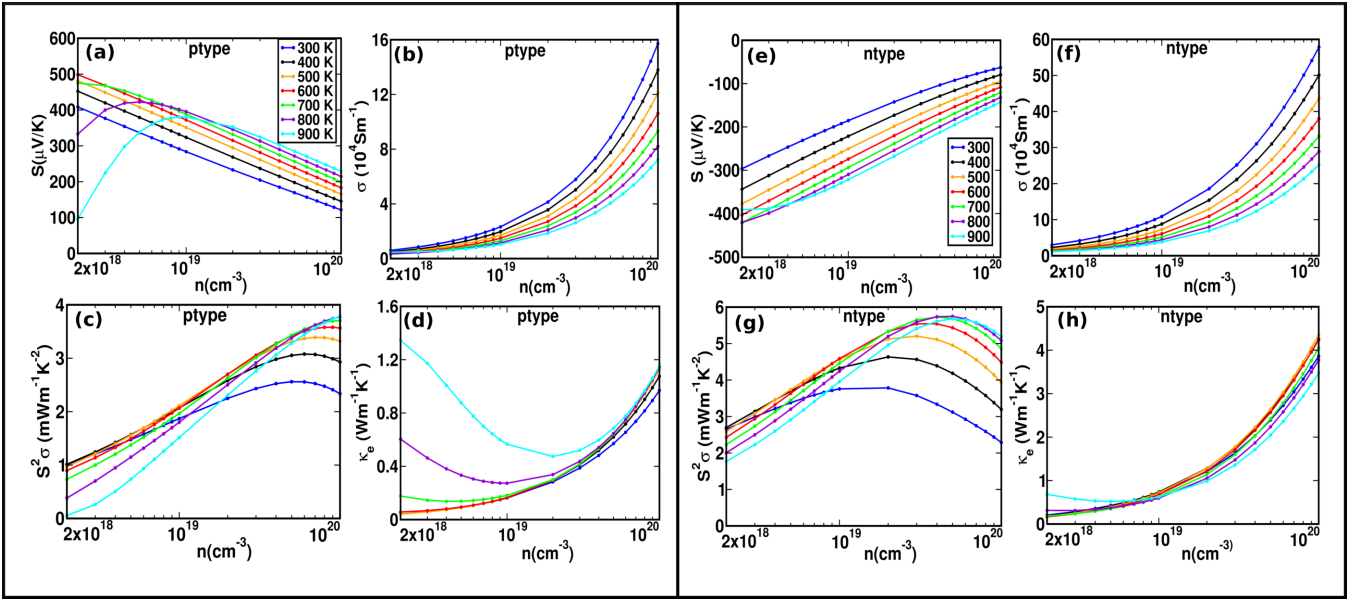


FIG. 4. For $\text{Cu}_2\text{ZnSiTe}_4$, carrier concentration (n) dependence of (a,e) Seebeck coefficient (S) (b,f) electrical conductivity (σ) (c,g) power-factor ($S^2\sigma$) and (d,h) electronic thermal conductivity (κ_e) for p-type (left) and n-type (right) conduction respectively at different temperatures (T).

for all three pairs Cu-Te, Zn-Te, and Si-Te. Similar electron localization around the Te atom is observed in case of Cu-Te and Zn-Te pairs, indicating an ionic bonding. On the other hand, Si-Te pair indicates a covalent-like bonding characteristic.

C. Electronic Transport

A temperature and energy dependent variable relaxation time approach is used to simulate the transport coefficients (S , σ and κ_e). This makes these quantities more accurate/reliable as compared to those simulated using constant relaxation time approximation (CRTA)³⁷⁻³⁹. In doped semiconductors, scattering mediated by ADP, POP and IMP play very crucial role. The variable relaxation time can be calculated using Fermi golden rule as,

$$\tau_{nk \rightarrow mk+q}^{-1} = \frac{2\pi}{\hbar} |g_{nm}(k, q)|^2 \delta(\epsilon_{nk} - \epsilon_{mk+q}) \quad (1)$$

where $g_{nm}(k, q)$ is the matrix element for scattering from state $|nk\rangle$ to state $|mk+q\rangle$ and ϵ_{nk} is the energy of the state $|nk\rangle$. Further details on the scattering specific matrix elements are discussed in Sec. II of SM³⁴. Figure 3 shows the carrier concentration (n) dependence of relaxation time (τ) at different temperatures for n- and p-type conduction. This relaxation time is calculated by incorporating the effect of all the four scatterings, i.e. ADP, POP, PIE and IMP. Relaxation times for each of the individual scatterings are shown in Fig. SII of SM³⁴. Total τ for p-type conduction varies between 55 and 13 fs in the entire concentration and temperature

range considered here, while the same for n-type conduction varies between 52 and 10 fs. Increasing temperature leads to a reduction in relaxation time due to the enhanced phonon scattering. Doping can be an efficient strategy to improve electrical conductivity. For example, excess Cu doping in $\text{Cu}_2\text{MnSnSe}_4$ is reported to increase the value of conductivity by 1 order of magnitude from 10^3 to 10^4 (S/m). Similarly, for n-type quaternary compound AgPbBiSe_3 ⁴⁰, conductivity value increases from 5×10^3 to 2.5×10^4 (S/m) with chlorine (Cl) doping. As such, for the power-factor ($S^2\sigma$) to enhance, the electrical conductivity should increase to such an extent that it can overcome the reduction in S , as a result of doping. To explore this, we have done calculations in the doping concentration range of 10^{18} - 10^{20} cm^{-3} . The effect of doping is incorporated within the rigid band approximation (RBA) which considers the topology of bands to remain intact as that of the parent system and vary the Fermi level in the band structure⁴¹. Seebeck coefficient values are found to be higher in p-type as compared to n-type conduction due to the flat valence bands. At high enough temperature, minority carriers may be generated which can affect the conduction mechanism, often known as bipolar thermal conduction. It is dominant at high temperatures and low carrier concentrations. Figure 4 shows the carrier concentration (n) dependence of S , σ , $S^2\sigma$ and electronic thermal conductivity (κ_e). Clearly, S decreases as n increases while σ follows the opposite trend which eventually helps to enhance power-factor ($S^2\sigma$). The latter approaches a maximum value at an optimal carrier concentration and then starts to decrease. Bipolar effect is visible at high temperatures and low n , which makes electronic thermal conductivity (κ_e)

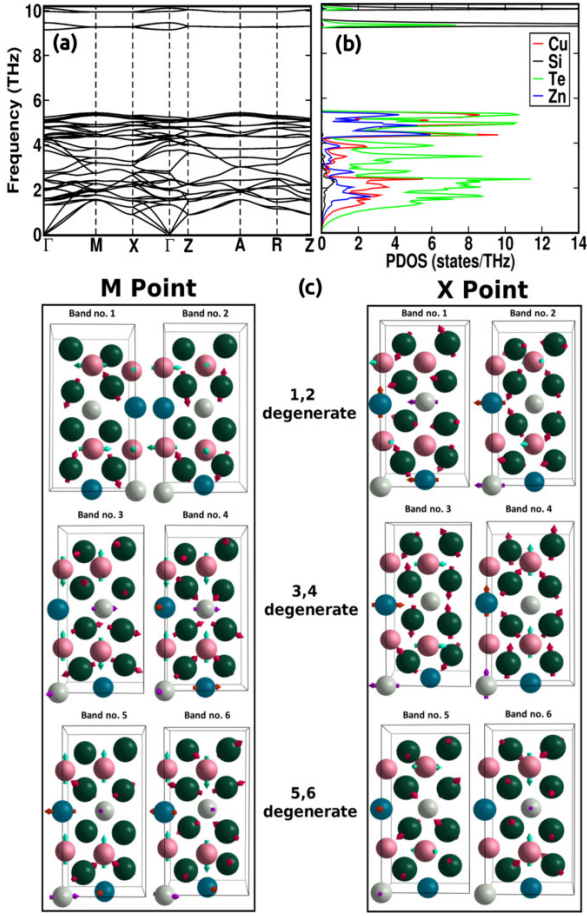


FIG. 5. For $\text{Cu}_2\text{ZnSiTe}_4$, (a) phonon dispersion (b) atom/orbital projected phonon density of states (PDOS) and (c) different phonon modes at M and X high symmetry points with band degeneracy.

increase in this regime. Clearly, peaks of TE coefficients occur at different carrier concentrations for n- and p-type conduction, which is due to the different nature of band topology resulting in different scattering rates.

The values of power-factor are comparable (or better) to some of the promising TE materials in this family Cu_2ABX_4 . $S^2\sigma$ for n-type conduction at 900 K is $3.95 \text{ mWm}^{-1}\text{K}^{-2}$ at the optimal carrier concentration of $1 \times 10^{19} \text{ cm}^{-3}$, which can be compared with $S^2\sigma = 0.5 \text{ mWm}^{-1}\text{K}^{-2}$ of Cl-doped AgPbBiSe_3 ⁴⁰. For p-type conduction, $S^2\sigma$ shows a peak value of $3.063 \text{ mWm}^{-1}\text{K}^{-2}$ at the optimal carrier concentration of $4 \times 10^{19} \text{ cm}^{-3}$, which can be compared with the Cu doped (excess) $\text{Cu}_2\text{MnSnSe}_4$ with the highest power-factor of $0.71 \text{ mWm}^{-1}\text{K}^{-2}$. Enhancement in electrical conductivity is predominantly responsible for such high values of power-factor.

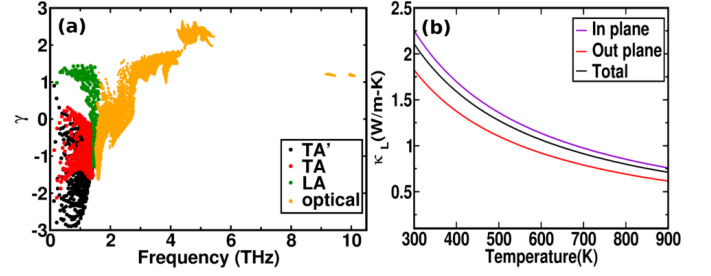


FIG. 6. For $\text{Cu}_2\text{ZnSiTe}_4$, (a) Gruneisen parameter (γ) vs. phonon frequency and (b) in-plane and out-of-plane component of lattice thermal conductivity (κ_L) vs. temperature.

D. Phonon properties

Figure 5(a) shows the phonon dispersion of $\text{Cu}_2\text{ZnSiTe}_4$. The low frequency acoustic phonons acquire small group velocity responsible for low lattice thermal conductivity. The group velocity for three acoustic branches LA, TA and TA' are 3306.96, 1717.18 and 2729.70 m/s respectively.

Mixing of low energy optical phonons with acoustic phonons enhances the phonon scattering leading to suppression of thermal transport. Te atom which resides in the tetrahedral void (surrounded by other atoms) vibrates in the free space of the void and scatters the phonon more. Nonetheless, the Te atom contributes dominantly to the low acoustic modes, as illustrated by the atom projected density of states in Fig. 5(b). The lowest optical branch which gets entangled with the acoustic branches lie at ~ 2 THz. Te atoms show appreciable contribution in this region as well, along with the Cu atoms. In the frequency range 4-6 THz, states of Te-atoms hybridize strongly with those of Cu and Zn, resulting in higher density of states and hence enhancement of phonon scattering. In order to show the nature of phonon propagation, we have plotted the eigen modes of different bands at two high symmetry points 'M' and 'X' in Fig. 5(c). It clearly shows the degeneracy of (1,2), (3,4) and (5,6) pairs of bands at these two high symmetry points. The first two degenerate modes are acoustic, 3rd and 4th bands are acoustic and optical respectively while the last two are optical modes. Appreciable mixing of acoustic and low lying optical phonon modes is responsible for the low lattice thermal conductivity, as discussed below.

Another important physical parameter that plays a crucial role in evaluating the lattice thermal conductivity is the Gruneisen parameter ($\gamma = -\frac{\partial \log \omega_i}{\partial V_i}$) which is also a measure of the degree of anharmonicity. Figure 6(a) shows the phonon frequency dependence of γ for different phonon modes. One can notice that γ is mostly positive in the higher frequency range, and shows negative values predominantly at low frequencies for acoustic modes. This implies that frequency will increase with the increase in volume. This might be due to the

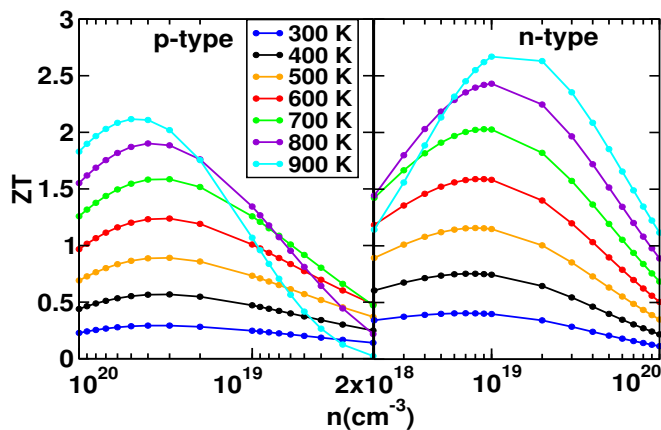


FIG. 7. For $\text{Cu}_2\text{ZnSiTe}_4$, carrier concentration (n) dependence of TE figure of merit (ZT) for p-type (left) and n-type (right) conduction respectively at different temperatures (T).

unique structure framework in the present case which consists of numerous cation-anion bonds, with the anion at the centre of the tetrahedral void (corner shared by cations). At low frequencies, transverse displacement of the anion (Te) atom causes a contraction of other cationic atoms towards each other in the void.⁴² Figure 6(b) shows the temperature dependence of calculated lattice thermal conductivity (κ_L). These calculations are done by incorporating inter-atomic force constants simulated up to third order which is expected to provide higher accuracy. Simulated κ_L is found to decrease from 2.1 to 0.7 $\text{Wm}^{-1}\text{K}^{-1}$ with increasing temperature from 300 to 900 K.

The κ_L values for few experimentally reported compounds belonging to this family such as $\text{Cu}_2(\text{Zn}/\text{Co}/\text{Mn}/\text{Fe})\text{SnSe}_4$ ^{10,12}, $\text{Cu}_2\text{HgSnTe}_4$ ¹¹ and $\text{Cu}_2(\text{Cd}/\text{Zn})\text{GeSe}_4$ ^{43,44} varies in the range 2.8 to 1.3 $\text{Wm}^{-1}\text{K}^{-1}$ at room temperature while reduces to the range 1.9 to 0.5 $\text{Wm}^{-1}\text{K}^{-1}$ at higher temperatures (600 to 800 K). Our calculated lattice thermal conductivity for $\text{Cu}_2\text{ZnSiTe}_4$ lie in a similar range. The theoretically reported κ_L values for few of the compounds belonging to the same family e.g. $\text{Cu}_2\text{CdSnTe}_4$ ⁴⁵ and $\text{CuZn}_2\text{InTe}_4$ ⁹ using Phono3py lie in the range 2.0 to 2.1 $\text{Wm}^{-1}\text{K}^{-1}$ at room temperature. After evaluating the electronic and

lattice thermal transport properties, we have estimated the ZT value for $\text{Cu}_2\text{ZnSiTe}_4$. Figure 7 depicts the carrier concentration dependence of ZT values at different temperatures. Our calculation shows reasonably high ZT values of 2.11 for p-type and 2.67 for n-type at $1 \times 10^{19} \text{ cm}^{-3}$ and $5 \times 10^{19} \text{ cm}^{-3}$ concentrations respectively at 900 K.

IV. Conclusions

In summary, we report a detailed study of the electronic and thermal transport properties of a quaternary chalcogenide $\text{Cu}_2\text{ZnSiTe}_4$ using first-principles calculation. This compound consists of two distinct structural units (Cu_2Te_4 and ZnSiTe_4) one of which is favourable for high electrical conduction while the other for thermal transport. In other words, it gives a flexibility to tune both types of conduction which is highly required for TE materials. The low band gap ($\sim 0.58 \text{ eV}$) along with large spin orbit coupling effects (due to Te-atoms) help to achieve reasonably high power factor, as large as ~ 3.95 and $3.06 \text{ mWm}^{-1}\text{K}^{-2}$ for n- and p-type conduction respectively. Distorted structural framework (involving cation-anion bonding, with anion at the centre of the tetrahedra void) helps to entangle the acoustic and low energy optical phonon modes, which in turn is responsible for reduced lattice thermal conductivity (lying in the range ~ 2.0 to $0.7 \text{ Wm}^{-1}\text{K}^{-1}$). Large power-factor and moderate κ_L values collectively make this compound a potential candidate for TE applications with TE figure of merit (ZT) ~ 2.11 (p-type) and 2.67 (n-type) at high temperature. We strongly believe that the present work can pave a path for future experimental studies on $\text{Cu}_2\text{ZnSiTe}_4$ for TE applications.

V. Acknowledgements:

HS and BS acknowledge the support of HPC facility (spacetime-2) at IIT Bombay. HS also acknowledges the computational support of the Thematic Unit of Excellence on Computational Materials Science, funded by the Nano Mission of the Department of Science and Technology at S N Bose National Centre for Basic Science, Kolkata. TSD acknowledges a J.C.Bose National Fellowship (grant no. JCB/2020/000004) for funding.

* aftab@iitb.ac.in

¹ Bo B. Iversen, Anders E.C. Palmqvist, David E. Cox, George S. Nolas, Galen D. Stucky, Nick P. Blake, and Horia Metiu. Why are Clathrates good candidates for thermoelectric materials? *J. Solid State Chem.*, 149(2):455–458, 2000. ISSN 0022-4596.

² M. Rull-Bravo, A. Moure, J. F. Fernández, and M. Martín-González. Skutterudites as thermoelectric materials: revisited. *RSC Adv.*, 5:41653–41667, 2015.

³ Kaiyang Xia, Chaoliang Hu, Chenguang Fu, Xinbing Zhao, and Tiejun Zhu. Half-Heusler thermoelectric materials.

Appl. Phys. Lett., 118(14):140503, 2021.

⁴ Bhakti Jariwala and Nuggehalli M. Ravindra. Process, property and performance of chalcogenide-based thermoelectric materials. *Nanomater. Energy*, 3(3):68–81, 2014.

⁵ Yixuan Shi, Cheryl Sturm, and Holger Kleinke. Chalcogenides as thermoelectric materials. *J. Solid State Chem.*, 270:273–279, 2019. ISSN 0022-4596.

⁶ Qijie Guo, Grayson M. Ford, Wei-Chang Yang, Bryce C. Walker, Eric A. Stach, Hugh W. Hillhouse, and Rakesh Agrawal. Fabrication of 7.2% efficient cztsse solar cells using czts nanocrystals. *J. Am. Chem. Soc.*, 132(49):17384–

- 17386, 2010.
- 7 G Nénert and T T M Palstra. Magnetolectric and multiferroic properties of ternary copper chalcogenides $\text{Cu}_2\text{MIINIVS}_4$. *J. Condens. Matter Phys.*, 21(17):176002, mar 2009.
 - 8 Ashmalina Rahman and Mohammad Mansoob Khan. Chalcogenides as photocatalysts. *New J. Chem.*, 45:19622–19635, 2021.
 - 9 Long Ma, Wencong Shi, and Lilia M. Woods. Structural diversity of Cu_2ZnSe_4 quaternary chalcogenides: electronic and phonon properties from first principles. *RSC Adv.*, 12: 26648–26656, 2022.
 - 10 Qingfeng Song, Pengfei Qiu, Feng Hao, Kunpeng Zhao, Tiansong Zhang, Dudi Ren, Xun Shi, and Lidong Chen. Quaternary pseudocubic $\text{Cu}_2\text{TMSnSe}_4$ (TM = Mn, Fe, Co) chalcopyrite thermoelectric materials. *Adv. Electron. Mater.*, 2(12):1600312, 2016.
 - 11 J. Navrátil, V. Kucek, T. Plecháček, E. Černošková, F. Laufek, Č Drašar, and P. Knotek. Thermoelectric properties of $\text{Cu}_2\text{HgSnSe}_4$ - $\text{Cu}_2\text{HgSnTe}_4$ solid solution. *J. Electron. Mater.*, 43(10):3719–3725, Oct 2014. ISSN 1543-186X.
 - 12 Ch. Raju, M. Falmbigl, P. Rogl, X. Yan, E. Bauer, J. Horky, M. Zehetbauer, and Ramesh Chandra Mallik. Thermoelectric properties of chalcogenide based $\text{Cu}_{2+x}\text{ZnSn}_{1-x}\text{Se}_4$. *AIP Advances*, 3(3):032106, 2013.
 - 13 Glen A. Slack. Thermal conductivity of ii-vi compounds and phonon scattering by Fe^{2+} impurities. *Phys. Rev. B*, 6:3791–3800, Nov 1972.
 - 14 Yi Xia, Vinay I. Hegde, Koushik Pal, Xia Hua, Dale Gaines, Shane Patel, Jiangang He, Muratahan Aykol, and Chris Wolverton. High-throughput study of lattice thermal conductivity in binary rocksalt and zinc blende compounds including higher-order anharmonicity. *Phys. Rev. X*, 10:041029, Nov 2020.
 - 15 Raju Chetty, Ashoka Bali, and Ramesh Chandra Mallik. Thermoelectric properties of indium doped $\text{Cu}_2\text{CdSnSe}_4$. *Intermetallics*, 72:17–24, 2016. ISSN 0966-9795.
 - 16 Min-Ling Liu, I-Wei Chen, Fu-Qiang Huang, and Li-Dong Chen. Improved thermoelectric properties of cu-doped quaternary chalcogenides of $\text{Cu}_2\text{CdSnSe}_4$. *Adv Mater*, 21(37):3808–3812, 2009.
 - 17 Teng Wang, Taichang Huo, Hongchao Wang, and Chunlei Wang. Quaternary chalcogenides: Promising thermoelectric material and recent progress. *Science China Materials*, 63(1):8–15, Jan 2020. ISSN 2199-4501.
 - 18 Qingfeng Song, Pengfei Qiu, Hongyi Chen, Kunpeng Zhao, Dudi Ren, Xun Shi, and Lidong Chen. Improved thermoelectric performance in nonstoichiometric $\text{Cu}_{2+x}\text{Mn}_{1-x}\text{SnSe}_4$ quaternary diamondlike compounds. *ACS Appl. Mater. Interfaces*, 10(12):10123–10131, 2018.
 - 19 Serghei Levchenko, Alexandr Nateprov, Victor Kravtsov, Maxim Guc, Alejandro Pérez-Rodríguez, Victor Izquierdo-Roca, Xavier Fontané, and Ernest Arushanov. Structural study and raman scattering analysis of $\text{Cu}_2\text{ZnSnSe}_4$ bulk crystals. *Opt. Express*, 22(S7):A1936–A1943, Dec 2014.
 - 20 W. Koshibae and S. Maekawa. Effects of spin and orbital degeneracy on the thermopower of strongly correlated systems. *Phys. Rev. Lett.*, 87:236603, Nov 2001.
 - 21 Ning Wang, Menglu Li, Haiyan Xiao, Zhibin Gao, Zijiang Liu, Xiaotao Zu, Sean Li, and Liang Qiao. Band degeneracy enhanced thermoelectric performance in layered oxyselenides by first-principles calculations. *Npj Comput. Mater.*, 7(1):18, Jan 2021. ISSN 2057-3960.
 - 22 G. Kresse and J. Furthmüller. Efficiency of ab-initio total energy calculations for metals and semiconductors using a plane-wave basis set. *Comput. Mater. Sci.*, 6(1):15–50, 1996. ISSN 0927-0256.
 - 23 G. Kresse and J. Furthmüller. Efficient iterative schemes for ab initio total-energy calculations using a plane-wave basis set. *Phys. Rev. B*, 54:11169–11186, Oct 1996.
 - 24 G. Kresse and J. Hafner. Ab initio molecular dynamics for liquid metals. *Phys. Rev. B*, 47:558–561, Jan 1993.
 - 25 John P. Perdew, Kieron Burke, and Matthias Ernzerhof. Generalized gradient approximation made simple. *Phys. Rev. Lett.*, 77:3865–3868, Oct 1996.
 - 26 Fabien Tran and Peter Blaha. Accurate band gaps of semiconductors and insulators with a semilocal exchange-correlation potential. *Phys. Rev. Lett.*, 102:226401, Jun 2009.
 - 27 Paolo Giannozzi and Stefano Baroni. Density-functional perturbation theory. pages 195–214, 2005.
 - 28 A Togo and I Tanaka. First principles phonon calculations in materials science. *Scr. Mater.*, 108:1–5, Nov 2015.
 - 29 Atsushi Togo, Laurent Chaput, and Isao Tanaka. Distributions of phonon lifetimes in brillouin zones. *Phys. Rev. B*, 91:094306, Mar 2015.
 - 30 Richard Dronskowski and Peter E. Bloechl. Crystal orbital hamilton populations (cohph): energy-resolved visualization of chemical bonding in solids based on density-functional calculations. *J. Phys. Chem.*, 97(33):8617–8624, 1993.
 - 31 Ryky Nelson, Christina Ertural, Janine George, Volker L. Deringer, Geoffroy Hautier, and Richard Dronskowski. Lobster: Local orbital projections, atomic charges, and chemical-bonding analysis from projector-augmented-wave-based density-functional theory. *J. Comput. Chem.*, 41(21):1931–1940, 2020.
 - 32 Stefan Maintz, Volker L. Deringer, Andrei L. Tchougréeff, and Richard Dronskowski. Analytic projection from plane-wave and paw wavefunctions and application to chemical-bonding analysis in solids. *J. Comput. Chem.*, 34(29): 2557–2567, 2013.
 - 33 Alex M. Ganose, Junsoo Park, Alireza Faghaninia, Rachel Woods-Robinson, Kristin A. Persson, and Anubhav Jain. Efficient calculation of carrier scattering rates from first principles. *Nat. Commun.*, 12(1), April 2021.
 - 34 See the supplementary material at [url] for more details on the effect of spin-orbit coupling on band structure, and formalism for calculation of carrier relaxation time and its variation with respect to temperature.
 - 35 Baisheng Sa, Zhimei Sun, and Bo Wu. The development of two dimensional group iv chalcogenides, blocks for van der waals heterostructures. *Nanoscale*, 8:1169–1178, 2016.
 - 36 Andreas Savin, Reinhard Nesper, Steffen Wengert, and Thomas F. Fässler. Elf: The electron localization function. *Angewandte Chemie International Edition in English*, 36(17):1808–1832, 1997.
 - 37 Shiqiang Hao, Logan Ward, Zhongzhen Luo, Vidvuds Ozolins, Vinayak P. Dravid, Mercouri G. Kanatzidis, and Christopher Wolverton. Design strategy for high-performance thermoelectric materials: The prediction of electron-doped KZrCuSe_3 . *Chem. Mater.*, 31(8):3018–3024, 2019.
 - 38 Sahib Hasan, Saro San, Khagendra Baral, Neng Li, Paul Rulis, and Wai-Yim Ching. First-principles calculations of thermoelectric transport properties of quaternary and ternary bulk chalcogenide crystals. *Materials*, 15(8), 2022.

ISSN 1996-1944.

- ³⁹ Koushik Pal, Xia Hua, Yi Xia, and Christopher Wolverton. Unraveling the structure-valence-property relationships in AMNQ₃ chalcogenides with promising thermoelectric performance. *ACS Appl. Energy Mater.*, 3(3):2110–2119, 2020.
- ⁴⁰ Moinak Dutta, Koushik Pal, Umesh V. Waghmare, and Kanishka Biswas. Bonding heterogeneity and lone pair induced anharmonicity resulted in ultralow thermal conductivity and promising thermoelectric properties in n-type AgPbBiSe₃. *Chem. Sci.*, 10:4905–4913, 2019.
- ⁴¹ Raimon S. The rigid-band model. *J. phys. radium , Phys. appl.*, 23(10):639–643, 1962.
- ⁴² Martin T Dove and Hong Fang. Negative thermal expansion and associated anomalous physical properties: review of the lattice dynamics theoretical foundation. *Reports on Progress in Physics*, 79(6):066503, may 2016.
- ⁴³ Raju Chetty, Jayaram Dadda, Johannes de Boor, Eckhard Müller, and Ramesh Chandra Mallik. The effect of Cu addition on the thermoelectric properties of Cu₂CdGeSe₄. *Intermetallics*, 57:156–162, 2015. ISSN 0966-9795.
- ⁴⁴ R. Chetty, A. Bali, O. E. Femi, K. Chattopadhyay, and R. C. Mallik. Thermoelectric properties of In-doped Cu₂ZnGeSe₄. *J. Electron. Mater.*, 45(3):1625–1632, Mar 2016. ISSN 1543-186X.
- ⁴⁵ Wencong Shi, Tribhuwan Pandey, Lucas Lindsay, and Lilia M. Woods. Vibrational properties and thermal transport in quaternary chalcogenides: The case of Te-based compositions. *Phys. Rev. Mater.*, 5:045401, Apr 2021.